Isolation of PD-L1 Extracellular Vesicle Subpopulations Using DNA Computation Mediated Microfluidic Tandem Separation

*Yinzhu Lu[+], Bingqian Lin[+], Weizhi Liu, Jialu Zhang, Lin Zhu, Chaoyong Yang and Yanling Song**

Abstract: Accurate isolation of targeted extracellular vesicle (EV) is challenging due to the heterogeneity of EV subpopulations which are from different cell origins. Most EV subpopulations lack a single marker whose expression cleanly distinguish them from mixed populations of closely related EVs. Herein, we developed a modular platform capable of taking multiple binding events as input, logic computations, and producing two independent outputs for tandem microchips for EV subpopulation isolation. Taking advantages of the excellent selectivity of dual-aptamer recognition-mediated DNA computation and the sensitivity of tandem microchips, this method achieves, for the first time, sequential isolation of tumour PD-L1 EVs and non-tumour PD-L1 EVs. As a result, the developed platform can not only effectively distinguish cancer patients from healthy donors, but also provides new clues for assessing immune heterogeneity. Moreover, the captured EVs can be released through a DNA hydrolysis reaction with high efficiency, which is compatible with downstream mass spectrometry for EV proteome profiling. Overall, this strategy is expected to isolate different EV subpopulations, translate EVs into reliable clinical biomarkers, and accurately investigate the biological functions of different EV subsets.

Extracellular vesicles (EVs) are released by almost all types of cells and are critical for intercellular communication[1]. EV subpopulations from different sources can accurately interact with their respective recipient cells, undergo internalization, and perform functions[1-2]. Therefore, separation of multiple EV subpopulations is necessary to fully understand EV biological functions.

Several techniques have been developed to isolate bulk EVs, including ultracentrifugation[3], microfluidic-based separation[4], size-based exclusion, and affinity-based isolation[3]. Of these methods, affinity-based separation is relatively selective and primarily relies on capturing EVs by interaction with a single associated biomarker[5]. These affinity-based strategies, although useful in some applications, are limited because most EV subpopulations lack a single marker whose expression cleanly distinguish them from mixed populations of closely related EVs. Dual-antibody based sandwich detection can improve some selectively, but this approach is difficult to execute when simultaneously attempting to isolate single and double markers expressing EV subpopulations[6].

The rapid development of DNA computation techniques based on aptamer recognition has offered a powerful tool for the deconvolution of heterogeneous EV subpopulations[7]. Multiple aptamers can be integrated for recognition of markers in close proximity to induce the subsequent logic computation and amplification[7]. Several aptamer-based computation methods have been developed for tumour-derived EV quantitation[8], and EV protein-specific glycosylation visualization[9]. However, considering the complexity of logical computation design as well as the high heterogeneity of EVs, the existing methods can only quantify one specific EV subpopulation at a time, but it is difficult to separate multiple EV subpopulations simultaneously. The lack of separation methods makes it difficult to achieve downstream analysis of multiple EV subpopulations, thus hindering the in-depth exploration of the biological functions and clinical application of EV subpopulations. Therefore, a separation strategy for multiple EV subpopulations is needed.

Inspired by precise EV-cell recognition via combinatorial recognition of multiple surface markers, we focused on tailored recognition-induced separation that exploits discriminatory combinatorial features of target EV subpopulations. To prove this concept, programmed death-ligand 1 (PD-L1) positive EVs of tumour-origin and non-tumour-origin were selected as targets. PD-L1 EVs were reported to mediate PD-1 immunosuppression and can be a tremendous potential marker of tumour diagnose[2, 10]. But the relative amounts of tumour-derived PD-L1 EVs and non-tumour-derived PD-L1 EVs (secreted by immune cells and mesenchymal stem cells) remain unknows due to the insufficiency in separation platforms. Taken together, the isolation and quantitation of PD-L1 EV subpopulations from different original sources can provide an effective reflection of tumour progress, and also yields new insight into how PD-L1 EV subpopulations function in immune regulation[11].

Towards this end, we developed a modular platform capable of taking multiple binding events as input, computing combinations of AND with NOT logic operations, and producing two independent outputs for tandem microfluidic separations (Scheme). For distinguishing PD-L1 EVs from tumour and non-tumour origins, a typically used tumour EV marker EpCAM (epithelial cell adhesion molecule)[12] was chosen for tumour-derived EV recognition. Two aptamers targeting EpCAM[13] and PD-L1[14] were designed as affinity probes with extension regions[15] for combinatorial recognition against tumour-derived PD-L1 EVs (Scheme A). Compared to an allosteric activation-based design, the extension-based probe design was better able to ensure the affinity and selectivity of the aptamer.

Only EVs co-expressing both EpCAM and PD-L1 induce the proximity of the two type probes, leading to increasing local concentrations of extension sequences for subsequent activation of the switch probe. To reduce the activation of switch probes by EVs expressing just one of the targets or probes in solution, the switch was designed is in a hairpin structure that uses a “latch” motif to sequester a complementary DNA (cDNA) of two extensions in an inactive mode until co-binding of combinatorial aptamer probes induces a conformational change. By labelling biotin on switches, biotin can be introduced onto tumour-derived PD-L1 EVs through combinatorial recognition mediated switch activation, while neither EV subpopulations expressing only one

Yinzhu Lu, Dr. Bingqian Lin, Weizhi Liu, Jialu Zhang, Dr. Lin Zhu, Prof. Yanling Song, Prof. Chaoyong Yang. The MOE Key Laboratory of Spectrochemical Analysis & Instrumentation, the Key Laboratory of Chemical Biology of Fujian Province, State Key Laboratory of Physical Chemistry of Solid Surfaces, Department of Chemical Biology, College of Chemistry and Chemical Engineering, Xiamen University, Xiamen, 361005, China.
E-mail: ylsong@xmu.edu.cn

Supporting information for this article is given via a link at the end of the document.

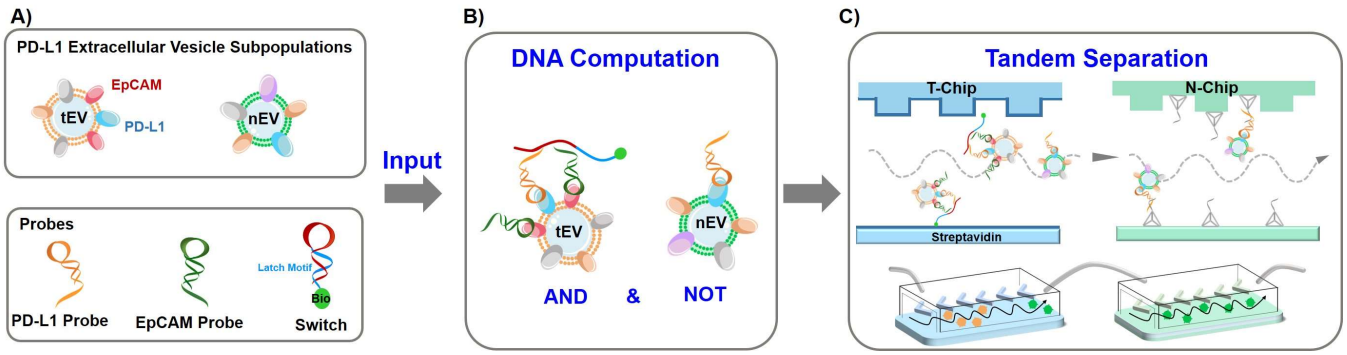

Scheme. Working principle of PD-L1 extracellular vesicle subpopulation isolation using DNA computation mediated-microfluidic separation. After incubation of the PD-L1 probe and the EpCAM probe, switch activated tumour cell-origin PD-L1 extracellular vesicle subpopulations (AND) and normal cell-origin PD-L1 extracellular vesicle subpopulations (NOT) were computed as input, and two independent outputs were processed by tandem microfluidic separations.

marker nor soluble proteins can trigger conformational changes of the switch (Scheme B). As a result, only tumour-derived PD-L1 EV populations can be isolated by streptavidin functioned microfluidic chip (T-Chip).

After the exclusion of tumour-derived PD-L1 EVs, the remaining PD-L1 EVs from normal cells can be captured via hybridization between the extension sequence on the PD-L1 probe and the corresponding cDNA modified on the second microfluidic chip (N-Chip) (Scheme C). Through utilization of combinatorial recognition-trigged computation and two tandem chips, the developed platform enables, sequential isolation and simultaneous quantification of tumour-derived PD-L1 EVs and normal cell derived PD-L1 EVs. In addition, after separation, tandem chips can be de-connected, so that the EV subpopulations on the corresponding chips can be respectively released by the nuclease for subsequent downstream analysis.

To achieve an optimal thermodynamic trade-off when two affinity probes efficiently hybridize with the switch only upon simultaneously affinity binding, we designed a series of the switches differing in the length of latch domains and probe extensions (Figure 1A, Table S1). Specifically, we designed extension domains of two affinity probes complementary to the switch with lengths ranging from 10 to 14 nucleotides (nt), while the intramolecular complementary length (latch domain) of the switch contained 7 or 8 nt.

Based on the simulated hybridization efficiency, there is a trade-off between the switch-extensions hybridization and the switch-single probe hybridization as the number of bases in the extended sequences increase (Figure 1B). In the serials of switches, switch 8-11-14 showed the best trade-off between responsiveness and selectivity (Figure S1). Then, the binding performance of switch 8-11-14 was verified by flow cytometry. The EVs derived from the human melanoma cells A375 (PD-L1+, EpCAM+) and the human glioma cell line U251 (PD-L1+, EpCAM-) were used as the model of tumour-derived PD-L1 EVs and normal-derived PD-L1 EVs, respectively (Figure S2). The EVs were incubated with single affinity probe or two affinity probes simultaneously, and then the switch. Specially, the group of dual affinity probes and switch 8-11-14 showed an obvious fluorescent shift against A375 EVs, whereas other groups with a single affinity probe and switch 8-11-14 showed no fluorescent shift compared to random sequence (Figure 1C, Figure S3). As for control U251 EVs, no fluorescent shift was observed in groups of both affinity probes or single affinity probes (Figure 1D). These results confirmed that only dual-recognition of two affinity probes, can induce the switch to open and bind to extended regions of two probes simultaneously.

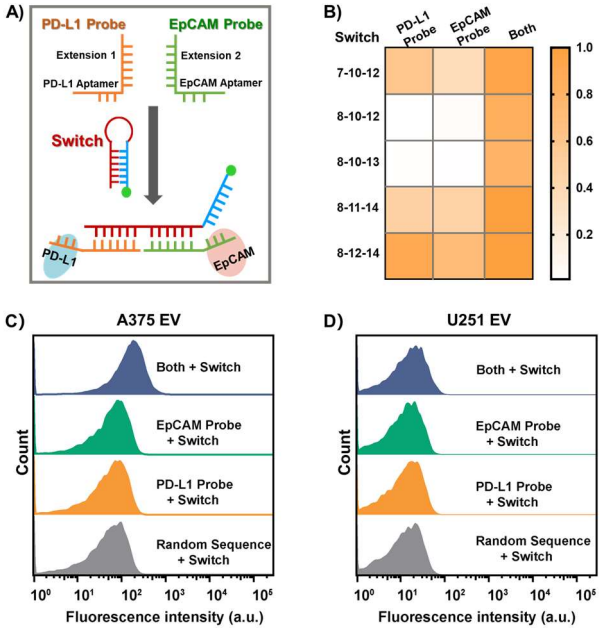

Figure 1. The design and validation of the switch probes. (A) The hairpin structure of the switch. Only co-binding of two affinity probes can induce a conformational change. The "latch" motif is blue. (B) The predicted hybridization ratios of the corresponding duplex by activation of a single affinity probe or dual affinity probes to a series of designed switches. The data were calculated by NUPACK™ Tool at 25℃. (C) Validation of switch 8-11-14 for PD-L1 and EpCAM dual-positive A375 EVs and (D) PD-L1 mono-positive U251 EVs.

We then evaluated the isolation performance of the AND logic computation triggered T-Chip. T-Chip was designed with the herringbone-shaped microchannel and modified by streptavidin (Figure 2A, Figure S4). The herringbone microfluidic chip can significantly accelerate mixing to increase collisions between EVs and the affinity interfaces. After incubating with the combination of affinity probes and biotin-labeled-switch, the A375 EVs were injected into the T-Chip and identified by CD63 antibody. And the signal was generated by the reaction of β-galactosidase conjugated secondary antibody and FDG (Figure S5). The probe concentration, flow rate, and beacon incubation time were optimized for better signal-to-background ratio (Figure 2B & C, Figure S6). As a consequence, by combinatorial recognition, logic calculation and T-Chip isolation, we obtained a response curve for different concentrations of PD-L1 from A375 EVs with a good

linear relation (R^2=0.97, LOD 4.79 pg/mL), suggesting that T-Chip can quantitatively detect tumour-derived PD-L1 EVs (Figure 2D). In contrast, T-Chip barely captures PD-L1 mono-positive U251 EVs, which demonstrates the great selectivity of T-Chip (Figure S7).

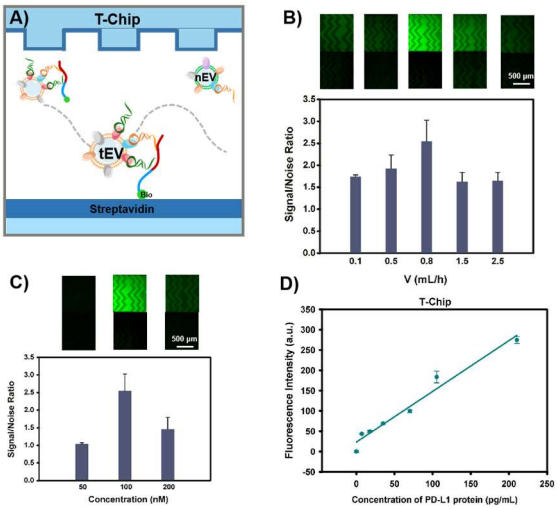

Figure 2. (A) The principle of T-Chip. (B) The optimization of flow rate and (C) probe concentration with corresponding fluorescence images. (D) The response curve for different concentrations of PD-L1 from A375 EVs with a good linear relation (R^2=0.97).

We next tested the potential of applying N-Chip for the detection of non-tumour-derived PD-L1 EVs. N-Chip was engineered on a tetrahedral DNA nano-scaffold (TDN) with a pendant cDNA probe at the top vertex. The nano-scale scaffold can prompt the cDNA probe in an ordered upright orientation, increasing the DNA hybridization kinetics and thermodynamics. As a result, normal cell-derived PD-L1 EVs with PD-L1, but not EpCAM expression, are bound only with the PD-L1 probe and can be captured by the N-Chip via the hybridization of cDNA and the extension domain of the PD-L1 probe (Figure 3A). The successful assembly of the cDNA-TDN was verified by polyacrylamide gel electrophoresis (Figure 3B). After the N-Chip was modified with cDNA-TDN probes, U251 EVs (PD-L1+, EpCAM-) were captured by N-Chip (Figure 3C). Moreover, the response curve also showed a good linear relation between the concentrations of PD-L1 from U251 EVs and the fluorescence intensity (Figure 3D), which verified the capture ability of N-Chip for non-tumour-derived PD-L1 EVs (R^2=0.96, LOD 8.58 pg/mL). Overall, these results verify the respective capture ability of T-Chip and N-Chip, indicating the possibility of serial separation of tumour and non-tumour derived PD-L1 expressed EVs by tandem microfluidic chips.

Then, the ability of tandem chips to separate different PD-L1 EV subpopulations was evaluated (Figure 4A). Mixtures of A375 EVs and U251 EVs in different proportions (1:0, 8:2, 2:8, 0:1) were analyzed by tandem T-Chip and N-Chip. The fluorescent intensity on each set of tandem chips is positive response to the captured EV amount. The calculated fluorescent ratios based on experimental results of T-Chip to N-Chip were 1:0, 82:18, 23:77 and 0:1 accordingly (Figure 4B), which were very close to the input ratio of two EV subpopulations. Moreover, the response curves of A375 EVs in T-Chip and U251 EVs in N- Chip were calculated as 0.98 and 0.99 respectively (Figure 4C&D). These results show that each chip can still maintain a good linear correlation when separating mixed PD-L1 EVs, which indicates good selectivity and great potential of the developed platform for EV subpopulation separation.

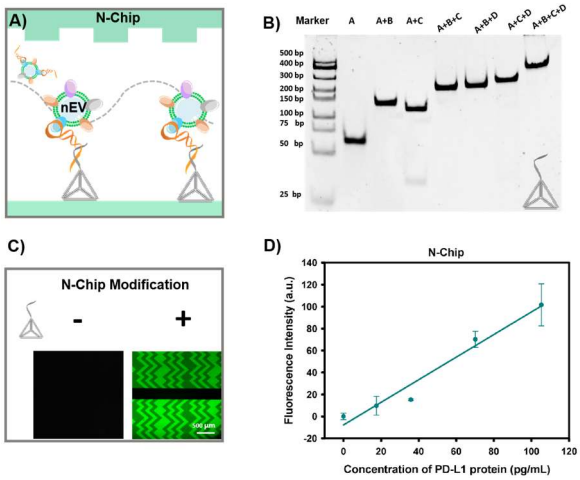

Figure 3. (A) The designed structure of tetrahedral DNA nano-scaffold with a pendant cDNA probe at the top vertex. (B) The validation of different stages of tetrahedral DNA assembly. (C) The fluorescence images of N-Chip for U251 EV enrichment. (D) The response curve for different concentrations of PD-L1 from U251 EVs with a good linear relation (R^2=0.96).

Beyond capture, EV subpopulation separation has an outstanding advantage over EV detection in terms of release of captured EVs for downstream analysis. Since both T-Chip and N-Chip were captured based on nucleic acid motifs, it is convenient to use nucleases to degrade DNA aptamers and switch probe for EV release (Figure S8). As a result, after dis-connected two tandem chips and incubation with DNase I for 15 min, about 83.7% and 78.8% captured EVs were released from the respective chips (Figure 5A, Figure S9A). Since this release strategy hydrolyzes DNA motifs rather than the protein expressed on the EV membrane, the topology and size of EVs were not changed significantly after release, suggesting the integrity of released EVs (Figure 5B & C, Figure S9B).

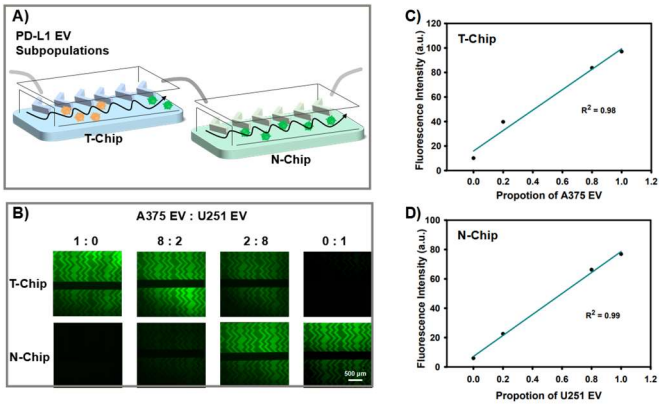

Figure 4. (A) Mixtures of A375 EVs and U251 EVs in different proportions are processed by tandem microfluidic separation. (B) The fluorescence images of Tumour-Chip and Normal-Chip in different proportions of A375 EVs and U251 EVs. (C) The response curve for different proportions of mixed EVs in T-Chip and (D) in N-Chip.

Moreover, mass spectrometry-based proteome profiling of EVs greatly contributes to the understanding of EV origin and function, and is critical for the development of exosomal biomarkers. To further explore the potential downstream application, we facilitated mass spectrometric identification and protein characterization of released EVs. As shown in Figure 5D & Figure S9C, after separation and release, there were 1295 and 1862 common proteins, and about 78.34% and 92.18% proteins of released EVs were consistent with A375 and U251 EVs before capture, respectively. Hence, this separation platform can not only quantify the content of different EV subpopulations, but also achieve protein profiles beyond the capability of detection-based platforms.

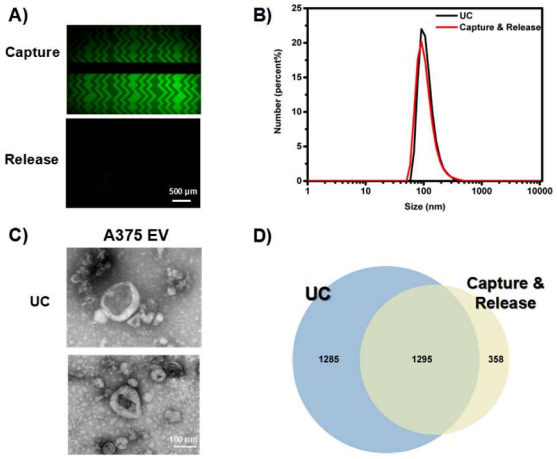

Figure 5. Validation of release capability of T-Chip. (A) The fluorescence images of T-Chip before and after the release of A375 EV. (B) The characterization of A375 EVs before and after release by DLS and (C) TEM. (D) The mass spectrometry-based proteome profiling of A375 EVs after isolation of ultracentrifugation and microfluidic separation. UC is short for ultracentrifugation.

Subsequently, plasma samples from a small cohort of lung cancer (Table S2) and healthy volunteers were used to investigate the clinical utility of the developed strategy. After two μL of plasma was diluted and incubated with affinity probes and the switch successively, then the mixture was injected into the tandem chips. As shown in Figure 6A, for T-Chip, the number of captured EVs from cancer patients was much higher than that of healthy volunteers (t test: P=0.0006). While for N-Chip, the distinction between the two types of samples was not obvious except for some healthy volunteers with high values (Figure 5B, t test: P = 0.02). It is worth noting that for the EVs isolated by N-Chip, the average amount of captured EVs from patients was lower than that of healthy people because the patient's PD-L1 EVs from normal cells may have been suppressed due to immune escape. If the signal intensities of the of the tandem microchips from the same sample were added together, the distinction between the patient and the normal would have been weakened (Figure 5C & D, t test: P = 0.04), because of the amount of PD-L1 EVs secreted by normal cells varies greatly due to the immunity heterogeneity. These results demonstrate that this strategy can distinguish cancer from normal people, but can also obtain the amount of PD-L1 EV subpopulations of normal cell origin to assist in the immunity assessment. This precise PD-L1 EV subpopulation isolation is expected to promote the conversion of the levels of PD-L1 EVs into reliable clinical biomarkers and exploration of comprehensive immunotherapy mechanisms.

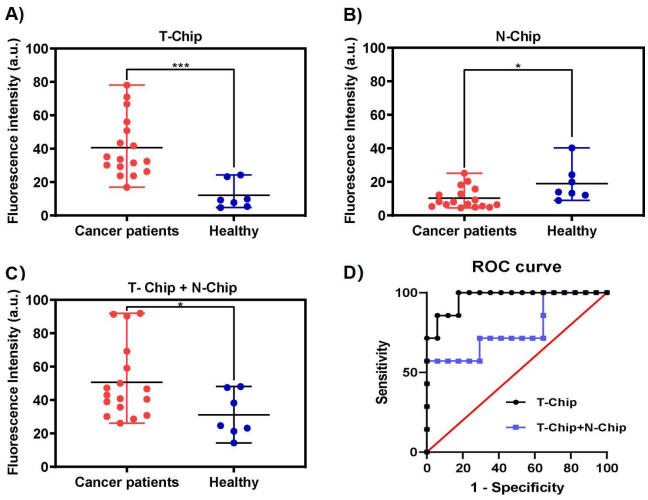

Figure 6. The separation of EVs from clinical samples by "AND" and "NOT" computation. (A) The separation of EVs from clinical samples only by T-Chip. (B) The separation of EVs from clinical samples only by N-Chip. (C) The separation of EVs from clinical samples was processed by tandem microfluidic separation. (D) The ROC curves of Tr-Chip only and tandem chips.

In conclusion, we have demonstrated EV subpopulation isolation through integration of dual-aptamer recognition-induced DNA computation and tandem microfluidic separation. This DNA logic mediated microfluidic separation enables, for the first time, sequential isolation of tumour PD-L1 EVs and non-tumour PD-L1 EVs. Furthermore, beyond the previous quantitative assays, this platform can achieve high efficiency and low destructive recovery of EV subpopulations through chip disconnection and DNA hydrolysis. The released EVs maintain a good topological structure and can be used for downstream protein profiling, thus paving the way toward molecular and functional analysis of EV subpopulations. Applying this platform to EVs in clinical serum samples, not only an accurate discrimination of cancer patients and healthy donors was archived by T-Chip, but also the immunity heterogeneity was demonstrated by N-Chip. While the isolation and clinical relevance of EV subpopulations is a relatively new direction, there is hope that the developed platform will allow an improved understanding of EV biological functions, cancer progression, immune response, and assessment of resistance to immunotherapy in real-time to improve clinical outcomes.

Acknowledgements

We thank the National Natural Science Foundation of China (22022409, 21735004, 21874089) for their financial support.

Keywords: Aptamer, EVs, Immunotherapy, Proximity ligation assay

References

[1] R. Kalluri, V. S. LeBleu, *Science* **2020**, *367*, eaau6977.
[2] F. T. Xie, M. X. Xu, J. Lu, L. X. Mao, S. J. Wang, *Mol. Cancer* **2019**, *18*.
[3] P. Li, M. Kaslan, S. H. Lee, J. Yao, Z. Gao, *Theranostics* **2017**, *7*, 789-804.
[4] a) J. C. Contreras-Naranjo, H. J. Wu, V. M. Ugaz, *Lab Chip* **2017**, *17*, 3558-3577; b) B. Q. Lin, Y. M. Lei, J. X. Wang, L. Zhu, Y. Q. Wu, H. M. Zhang, L. L. Wu, P. Zhang, C. Y. Yang, *Small Methods* **2021**, *5*.

[5] a) N. Zarovni, A. Corrado, P. Guazzi, D. Zocco, E. Lari, G. Radano, J. Muhhina, C. Fondelli, J. Gavrilova, A. Chiesi, *Methods* **2015**, *87*, 46-58; b) H. Y. Xu, C. Liao, P. Zuo, Z. W. Liu, B. C. Ye, *Anal. Chem.* **2018**, *90*, 13451-13458; c) S. S. Kanwar, C. J. Dunlay, D. M. Simeone, S. Nagrath, *Lab Chip* **2014**, *14*, 1891-1900.

[6] P. Sharma, S. Ludwig, L. Muller, C. S. Hong, J. M. Kirkwood, S. Ferrone, T. L. Whiteside, *J. Extracell. Vesicles* **2018**, *7*.

[7] L. L. Chen, W. Z. Chen, G. Liu, J. Y. Li, C. H. Lu, J. Li, W. H. Tan, H. H. Yang, *Chem. Soc. Rev.* **2021**, *50*, 12551-12575.

[8] a) B. Q. Lin, T. Tian, Y. Z. Lu, D. Liu, M. J. Huang, L. Zhu, Z. Zhu, Y. L. Song, C. Y. Yang, *Angew. Chem. Int. Ed.* **2021**, *60*, 7582-7586; b) Y. K. Li, J. Q. Deng, Z. W. Han, C. Liu, F. Tian, R. Xu, D. Han, S. H. Zhang, J. S. Sun, *J. Am. Chem. Soc.* **2021**, *143*, 1290-1295.

[9] a) M. J. Huang, L. Zhu, S. Y. Kang, F. D. Chen, X. Y. Wei, L. Y. Lin, X. F. Chen, W. Wang, Z. Zhu, C. Y. Yang, Y. L. Song, *Anal. Chem.* **2021**, *93*, 15958-15963; b) L. Zhu, Y. F. Xu, X. Y. Wei, H. T. Lin, M. J. Huang, B. Q. Lin, Y. L. Song, C. Y. Yang, *Angew. Chem. Int. Ed.* **2021**, *60*, 18111-18115; c) Y. N. Guo, J. Tao, Y. R. Li, Y. M. Feng, H. X. Ju, Z. F. Wang, L. Ding, *J. Am. Chem. Soc.* **2020**, *142*, 7404-7412.

[10] a) G. Chen, A. C. Huang, W. Zhang, G. Zhang, M. Wu, W. Xu, Z. Yu, J. Yang, B. Wang, H. Sun, *Nature* **2018**, *560*, 382-386; b) M. Poggio, T. Hu, C.-C. Pai, B. Chu, C. D. Belair, A. Chang, E. Montabana, U. E. Lang, Q. Fu, L. Fong, *Cell* **2019**, *177*, 414-427. e413; c) Y. Tang, P. Zhang, Y. Wang, J. Wang, M. Su, Y. Wang, L. Zhou, J. Zhou, W. Xiong, Z. Zeng, *Front. Immunol.* **2020**, *11*, 604.

[11] D. Daassi, K. M. Mahoney, G. J. Freeman, *Nat. Rev. Immunol.* **2020**, 1-7.

[12] C. Patriarca, R. M. Macchi, A. K. Marschner, H. Mellstedt, *Cancer Treat. Rev.* **2012**, *38*, 68-75.

[13] Y. Song, Z. Zhu, Y. An, W. Zhang, H. Zhang, D. Liu, C. Yu, W. Duan, C. J. Yang, *Anal. Chem.* **2013**, *85*, 4141-4149.

[14] M. Huang, J. Yang, T. Wang, J. Song, J. Xia, L. Wu, W. Wang, Q. Wu, Z. Zhu, Y. Song, *Angew. Chem. Int. Ed.* **2020**, *132*, 4830-4835.

[15] S. Fredriksson, M. Gullberg, J. Jarvius, C. Olsson, K. Pietras, S. M. Gústafsdóttir, A. Östman, U. Landegren, *Nat. Biotechnol.* **2002**, *20*, 473-477.